

10. Hilde, T. W. C. et al. *Tectonophysics* **38**, 145–165 (1977).
11. Schwartz, D., Gill, J. B. & Silver, E. A. *EOS* **64**, 872 (1983).
12. Silver, E. A., Gill, J. B., Schwartz, D., Prasetyo, H. & Duncan, R. A. *Geology* **13**, 687–691 (1985).
13. Parsons, B. & Sclater, J. G. *J. geophys. Res.* **82**, 803–827 (1977).
14. Sclater, J. G. et al. *J. geophys. Res.* **81**, 309–318 (1976).
15. Watanabe, T. et al. *Maurice Ewing Ser. Am. geophys. Un.* **1**, 137–161 (1977).
16. Hamilton, W. *Prof Pap. U.S. geol. Surv.* No. 1078, 1–345 (1979).
17. Karig, D. E. *Tectonics* **2**, 211–236 (1983).
18. McCabe, R. et al. *Circum-Pacific Coun. Energy Miner. Res.* **1**, 421–436 (1985).
19. Hawkins, J. W. et al. *Circum-Pacific Coun. Energy Miner. Res.* **1**, 437–463 (1985).
20. Hsu, I. *thesis*, Washington Univ. (1972).
21. McCabe, R. *Tectonics* (in the press).
22. Louden, K. *J. geophys. Res.* **82**, 2989–3002 (1977).
23. Taylor, B. & Hayes, D. E. *Monogr. Am. geophys. Un.* **27**, 23–56 (1983).
24. Holloway, N. H. *Bull. Am. Ass. petrol. Geol.* **66**, 1355–1383 (1981).
25. Haile, N. S. & Wang, N. P. *Mem. Malay. geol. Surv.* **16**, 1–199 (1965).
26. Sukamoto, R. & Simandjuntak, T. O. *Bull. geol. Res. Dev. Cent.* **7**, 1–12 (1983).
27. Silver, E. A. et al. *J. geophys. Res.* **83**, 1681–1691 (1983).
28. Visser, W. A. & Hermes, J. J. *Verh. K. Ned. Geol.-mijnb. Genoot* **20**, 1–265 (1962).
29. Audley-Charles, M. G. *Geol. Mag.* **102**, 267–272 (1968).
30. Schouten, H. & McCamy, K. *J. geophys. Res.* **77**, 7089–7099 (1972).

Seismic measurements reveal a saturated porous layer beneath an active Antarctic ice stream

D. D. Blankenship, C. R. Bentley,
S. T. Rooney & R. B. Alley

Geophysical and Polar Research Center,
University of Wisconsin-Madison,
1215 West Dayton Street, Madison, Wisconsin 53706, USA

Seismic reflection studies recently conducted on ice stream B, part of the marine ice sheet of West Antarctica, show a metres-thick layer immediately beneath the ice in which both compressional (P) and shear (S) wave speeds are very low. These low wave speeds imply that the material in the layer is highly porous and is saturated with water at a high pore pressure. From this, and from arguments presented in an accompanying paper¹ to the effect that the layer would be too weak to support the shear stress exerted by the overlying ice, we conclude that the layer is deforming and that the ice stream probably moves principally by such deformation.

For the past decade, the stability of marine ice sheets (ice sheets grounded below sea level) has stood as a fundamental unsolved problem in glaciology. In particular, the West Antarctic ice sheet has been of concern because of the possibility that it might shrink rapidly in response to climatic warming, thus raising sea level by ~5 m. But no understanding of the dynamics of the West Antarctic ice sheet is possible until the processes and interactions that govern the development and movement of ice streams, by far the most active parts of the ice sheet, are understood.

Consequently, a major program was initiated in 1983 to study the West Antarctic ice streams that feed into the Ross Ice Shelf and their interaction with that ice shelf. One aspect of this program is a concentrated geophysical study at a site on ice stream B (Fig. 1), aimed at learning more about the nature of the contact zone between the ice stream and its bed, because in this zone lies the crucial determinant of ice movement. Glaciologists agree that water lubrication must be an important factor in allowing ice streams to move so rapidly despite small driving stresses (small surface slopes), but just how the water effects the rapid sliding—whether it acts through the mechanism of a thin, approximately uniform sheet, through channels incised in the underside of the ice, or through some other mechanism—is not known^{2–6}.

The field survey during the first season of the program (1983–84) comprised seismic recordings at ~300 sites along three lines at angles of 60° to one another, over an area of ~10 km². Geophone spreads were generally ~720 m long, with 30-m geophone spacings. All three components of motion were recorded so as to yield both P-wave and S-wave arrivals. Shots ranging

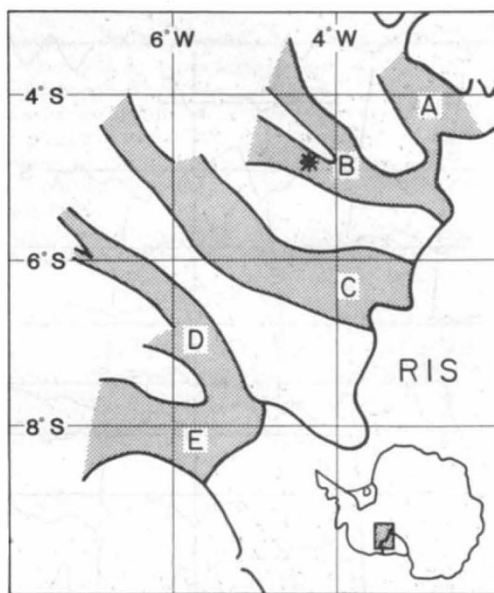


Fig. 1 Location map of ice streams along the Siple Coast of West Antarctica. An index map of Antarctica is in the lower right-hand corner. RIS, Ross Ice Shelf. Stippled areas are ice streams; the measurement site on ice stream B is marked by an asterisk. Standard grid coordinates are shown: in this rectangular system, 0° of longitude lies along the Greenwich meridian; and 0° of latitude passes through the South Pole.

in size from 0.15 to 0.45 kg were fired in shot holes ~20 m deep at spread centres and at various distances up to 4 km from the ends of the spreads. All the data were recorded on a digital recording system which was designed and built at the Geophysical and Polar Research Center. The system has a dynamic range of 84 dB and, for these experiments, sampled each of 24 channels at 0.4-ms intervals.

The existence of two reflectors near the base of the ice is seen very clearly in the seismogram of Fig. 2. In this example, the second echo is actually stronger than the first. The entire double-echo pattern is repeated 21 ms later in secondary ('ghost') seismic waves that have travelled upward from the shot to be reflected first from the surface of the glacier and then from the bed. All of the travel times in Fig. 2 have been reduced for 'normal move-out', so that reflections from a flat, level surface

Table 1 Porosities calculated by comparing v_p as measured on ice stream B with laboratory measurements

Sample	f (kHz)	Δv_p (m s ⁻¹)	Porosity	Ref.
Sand	1,000	100	0.38 ± 0.10	11
Variety of marine sediments	200	35	0.45 ± 0.18	12
Clayey silt	400	10	0.38 ± 0.10	13
Shallow water clayey silt	400	10	0.39 ± 0.09	13
Lake Erie sediments	330	0	0.41 ± 0.13	14
Artificial sands	250	100	0.33 ± 0.07	15
Unweighted mean				0.39 ± 0.06

f is the frequency in the laboratory measurements, and Δv_p is the velocity correction relative to low frequency. Error figures on porosities correspond to a velocity uncertainty of ± 120 m s⁻¹, compounded, in an r.m.s. sense, of the uncertainty in measured velocity of ± 100 m s⁻¹, and assumed uncertainty in Δv_p of ± 50 m s⁻¹, and a characteristic r.m.s. scatter in the laboratory data of ± 40 m s⁻¹. We use an unweighted mean because we view all of the standard deviations as equally valid estimates of a single value applicable to all the measurements.

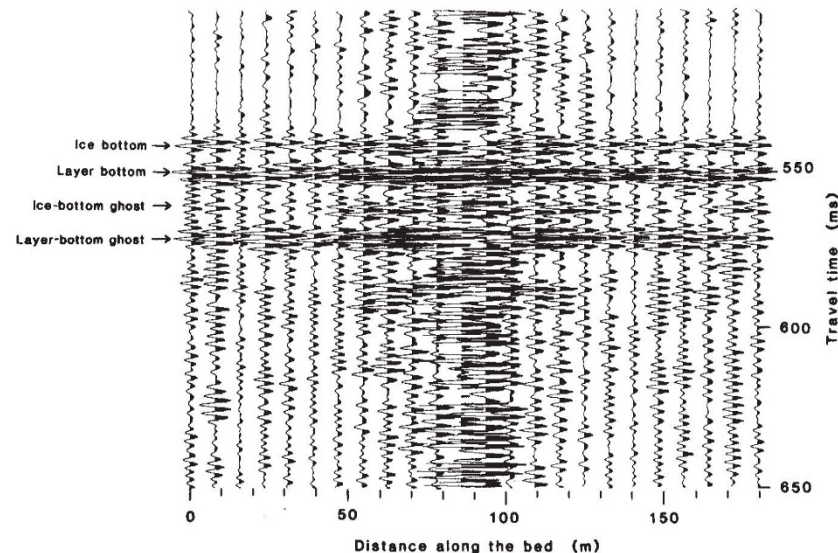


Fig. 2 Seismogram showing ice-bottom, layer-bottom, and ghost echoes, as marked. All traces have been adjusted for 'normal move-out'.

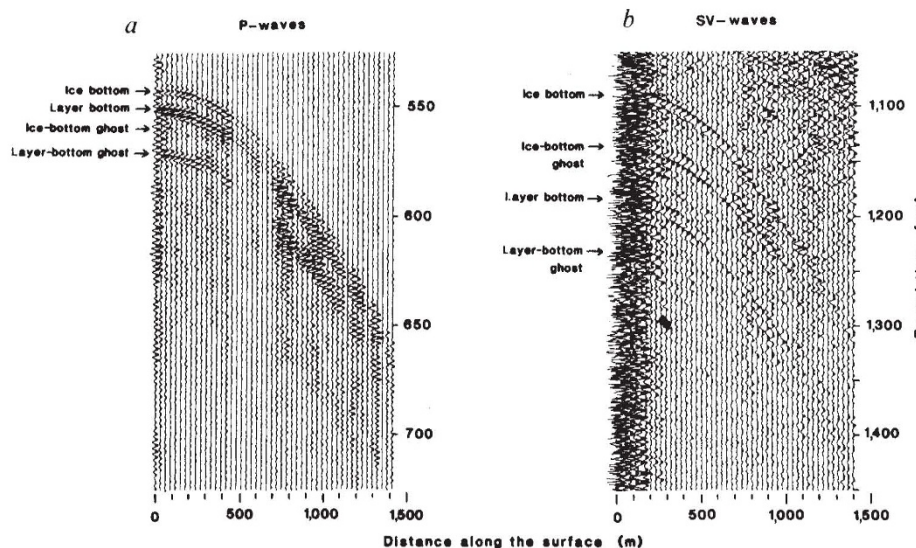


Fig. 3 Sequences of seismograms depicting 'wide-angle' (oblique) reflections. Not corrected for normal move-out. *a*, P-wave reflections; *b*, SV-wave reflections.

will appear at the same time regardless of the different horizontal distances between the shot and the various geophones.

The seismogram of Fig. 2, which was recorded along a direction parallel to the ice movement, depicts two level, coherent, reflecting surfaces separated by a travel-time difference (δt) of 10 ms. At a P-wave speed (v_p) in the layer of $1,600 \text{ m s}^{-1}$, that value of δt corresponds to a layer 8 m thick.

The wave speed in the layer was determined by means of 'wide-angle' (oblique) reflections over the section shown in Fig. 2. (The change in the travel-time difference between the two reflections as the shot and detectors are moved symmetrically outwards from the centre in opposite directions is a measure of the wave speed between the two reflectors.) The wide-angle profile (Fig. 3*a*) reveals that there is little change in the reflection-time difference between the two reflectors, which means that v_p in the layer is low compared with v_p in the ice ($3,830 \text{ m s}^{-1}$). Thus, we are not seeing a basal layer within the ice. Numerical inversion of the wide-angle travel times yielded $v_p = 1,600 \pm 100 \text{ m s}^{-1}$ in the layer. This precision was made possible by the large signal-to-noise ratio and the high frequency of the echoes, which permitted a timing precision of 0.2 ms. The inversion procedure fully considers the dip of both the top and bottom of the layer as well as the ray bending caused by the vertically inhomogeneous velocity structure near the surface of

the ice stream.

S-wave reflections from the upper and lower surfaces of the layer were recorded also (Fig. 3*b*), but with a δt that is 11 times as great as that for P-waves. This indicates an S-wave speed (v_s) of only $150 \pm 10 \text{ m s}^{-1}$ in the layer. In the Earth, v_s values this low are found only in very porous material under low effective (differential) pressure (the difference between the overburden pressure, which tends to force the grains more tightly together and thus increase the rigidity of the solid framework of the sediment, and the pore-water pressure, which tends to weaken the contact between the grains). Beneath ice stream B this must mean a saturated sediment, in which the weight of the thousand metres of overlying ice is supported principally by the pore fluid.

Along the direction of ice movement the subglacial reflecting horizons are clearly parallel to the ice bottom (Fig. 4*a*). The occurrence of more than one reflector suggests some stratification within the layer; the indicated strata are all nearly flat in the upstream-downstream direction. Transverse to the ice movement, however, there is much less continuity in the subglacial reflectors, and several sloping features appear (Fig. 4*b*). Most striking is the hump, occurring at $\sim 0.8 \text{ km}$ along the profile, that seems to rise near, or even to, the base of the ice. Since no deeper reflectors can be seen, it appears that,

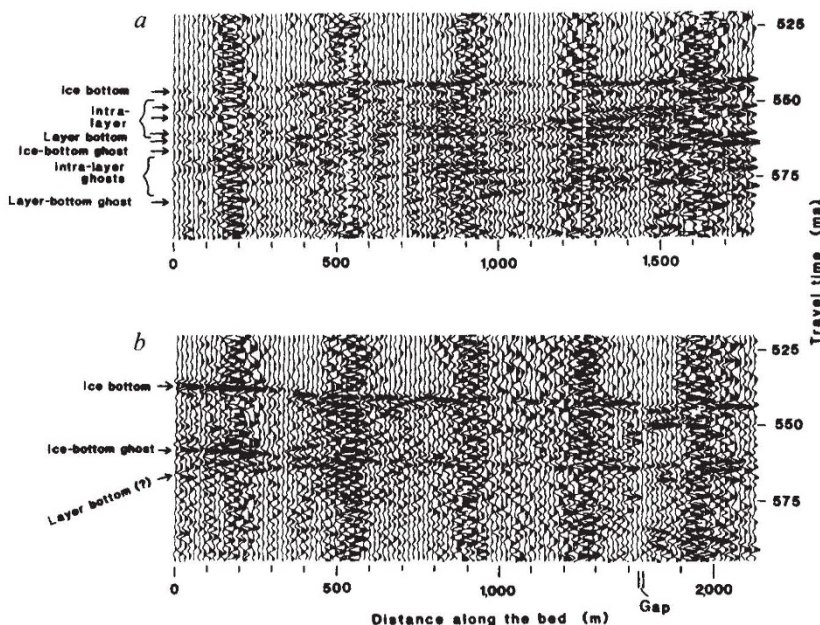


Fig. 4 Seismic reflection sections, each comprising five individual seismograms. Corrected for normal move-out. *a*, Section parallel to direction of ice movement; *b*, section transverse to ice movement.

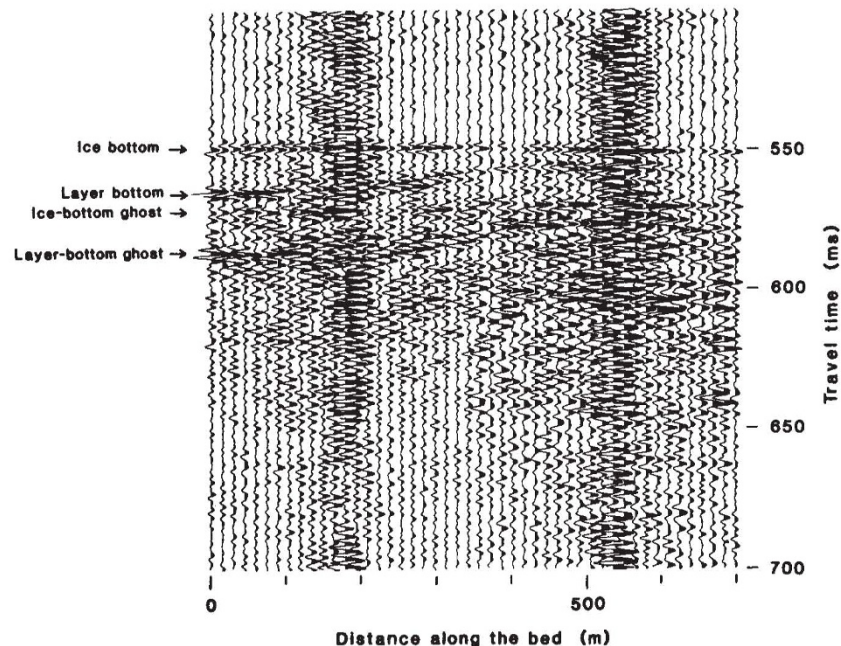


Fig. 5 Seismic reflection section transverse to ice movement, comprising two individual seismograms. Corrected for normal move-out.

locally, the layer nearly or entirely pinches out. Another section transverse to the ice stream (Fig. 5) shows a coherent layer-bottom reflection across the entire 0.8 km with a clear topographic relief of 8 m (10 ms). The maximum layer thickness on this section is 12 m (15 ms). From the available data we estimate an average thickness of 5 or 6 m.

The picture that emerges from the longitudinal and transverse sections is one of ridges and valleys in the basal surface of the sub-glacial layer, trending parallel to the axis of the ice stream. The alignment of these features along the direction of movement suggests that they are formed by erosion. It is significant to our model of a deforming bed¹ that there is no reflection of the ridges and troughs in the glacial/sub-glacial interface.

In a porous, saturated sediment, v_p depends primarily on the porosity n (and therefore the density), whereas v_s is most sensitive to the effective pressure ΔP . We can therefore estimate both n and ΔP using the v_p and v_s we have observed for the layer. Because $v_s \ll v_p$, both the rigidity and the incompressibility of the sedimentary frame are small compared with the bulk incom-

pressibility, κ , which then can be expressed simply as $\kappa = [(1-n)\beta_s + n\beta_w]^{-1}$, wherein β_s and β_w are the compressibilities of the sedimentary particles and the water, respectively. For a typical rock particle, we take $\beta_s = 2.6 \times 10^{-11} \text{ m}^2 \text{ N}^{-1}$, and for fresh water at 0 °C, $\beta_w = 5.0 \times 10^{-10} \text{ m}^2 \text{ N}^{-1}$. From the seismic measurements, on the other hand, $\kappa = \rho v_p^2$, where the bulk sediment density $\rho = (1-n)\rho_s + n\rho_w$; ρ_s is the density of the sedimentary particles and ρ_w is the density of fresh water. We take $\rho_s = 2.6 \times 10^3 \text{ kg m}^{-3}$ and $\rho_w = 10^3 \text{ kg m}^{-3}$. Equating the two expressions for κ , we obtain $n = 0.365 \pm 0.075$ for $v_p = 1,600 \pm 100 \text{ m s}^{-1}$.

Comparisons can also be made with laboratory and *in situ* measurements of v_p versus n in saturated sediments, but two corrections are needed. First, because most of the published values of v_p refer to sediments saturated with sea water and are corrected approximately to standard laboratory temperature and pressure, we must add a correction of 100 m s^{-1} (ref. 7) to our measured velocity, which refers to fresh water at 0 °C and a glaciostatic pressure of 9 MPa.

Table 2 Effective pressures (ΔP) calculated by comparing v_s as measured on ice stream B with laboratory measurements

Sample	ΔP (kPa)	Ref.
Artificial sand	40 ± 5	15
Silt	60 ± 5	16
Silty clay	30 ± 5	16
Potter's clay	120 ± 5	16
Marine silt-clays	70 ± 50	17*
Angular-grained material	15 ± 5	17†
Sands	25	18
Clays and silts	60	18
Unweighted mean	50 ± 40	

Error figures for ΔP correspond directly to a velocity uncertainty of $\pm 10 \text{ m s}^{-1}$ except in the case of the marine silt-clays¹⁷, for which a range of observed curves was taken into account. In calculating the standard error estimate for the mean, we have assumed a standard deviation of $\pm 50 \text{ kPa}$ in ΔP for each sample.

* From Fig. 2 in ref. 17, using the supplementary relation: depth = $\Delta P / (\rho - \rho_w)g$, where g is the acceleration of gravity.

† From equation (6) in ref. 17.

Second, most laboratory measurements are made at frequencies between 100 kHz and 1 MHz, whereas our seismic frequencies are only $\sim 400 \text{ Hz}$. Standard Biot theory^{8,9} with $n = 0.4$ (to be justified below) leads to a limiting high-frequency wave speed that is $\sim 100 \text{ m s}^{-1}$ higher than the low-frequency speed. We have, therefore, added to our field measurements approximate frequency-effect corrections (Δv_p in Table 1) calculated according to standard theory¹⁰. These corrections are in approximate agreement with those measured for 1 MHz for various sediments⁹, but because Δv_p depends on permeabilities in the sediment samples that had to be estimated, we assume an uncertainty in Δv_p of $\pm 50 \text{ m s}^{-1}$. Fuller details will be given elsewhere.

The porosities obtained from these comparisons show considerable scatter (Table 1) but are in satisfactory agreement with the value calculated above by linearly combining compressibilities and densities. It therefore seems safe to conclude that n in the sub-glacial layer is close to 0.4, although probably a bit less. That is close to 0.4 and not 0.3 or less is significant, as it strongly suggests that the sub-glacial material is dilated and deforming¹.

From v_p and ρ in the layer we can calculate that the acoustic impedance of the sediment is close to that of the ice. This explains how the echo from the bottom of the sediment could be stronger than that from the base of the ice. Echo amplitudes vary widely over the survey area, however; they will be considered in detail elsewhere.

The other quantity we wish to estimate is ΔP , since it is critical to the shear strength of the medium. The best measure of ΔP is v_s , because in an unconsolidated sediment v_s depends principally on the intergranular friction, and therefore on the intergranular pressure. Again, comparison with several experimental values leads to a considerable uncertainty (Table 2); nevertheless, all estimates of ΔP lie in the range 15–120 kPa. We adopt the mean value of $50 \pm 40 \text{ kPa}$ for ΔP in the sub-glacial layer.

We conclude that at least at one location, an active Antarctic ice stream is underlain by a layer of saturated sediment ranging in thickness from zero or nearly zero to at least 12 m, with an average of 5 or 6 m. The layer varies much less in thickness parallel to the direction of ice movement than normal to it; because its upper surface is planar, this gives the impression of a series of longitudinal grooves in the substrate beneath the layer. The low seismic wave speeds in the layer indicate that the material has a porosity of ~ 0.4 and is saturated with water at a pore pressure only $\sim 50 \text{ kPa}$ less than the glaciostatic pressure (9 MPa). Because these characteristics imply that the sub-glacial material is very weak¹, we believe that the sub-glacial

layer is deforming and eroding the stationary surface below, and that it is deformation within the layer rather than deformation in the ice or basal sliding that is the principal component of ice-stream movement.

The field program is a cooperative effort among investigators from the University of Wisconsin, the Ohio State University, NASA and the University of Chicago. We thank B. R. Weertman, J. E. Nyquist, R. Flanders, S. Shabtaie, D. G. Schultz, K. C. Taylor, Jr and J. Dallman for help with field work, L. A. Powell, B. D. Karsh, R. B. Abernathy, W. L. Unger, and Weertman for engineering assistance, and A. N. Mares and S. H. Smith for manuscript and figure preparation. Financial support was provided by NSF under grants DPP81-20322 and DPP84-12404. This is contribution number 447 of the University of Wisconsin-Madison, Geophysical and Polar Research Center.

Received 23 December 1985; accepted 15 April 1986.

- Alley, R. B., Blankenship, D. D., Bentley, C. R. & Rooney, S. T. *Nature* **322**, 57–59 (1986).
- Iken, A. *J. Glaciol.* **27**, 407–421 (1981).
- Weertman, J. & Birchfield, G. E. *Ann. Glaciol.* **3**, 316–320 (1982).
- Bindschadler, R. J. *J. Glaciol.* **29**, 3–19 (1983).
- Iken, A., Rothlisberger, H., Flotron, A. & Haeberli, W. *J. Glaciol.* **29**, 28–47 (1983).
- Kamb, B. *et al. Science* **227**, 469–479 (1985).
- Clay, C. S. & Medwin, H. *Acoustical Oceanography: Principles and Applications* (Wiley, New York, 1977).
- Biot, M. A. *J. acoust. Soc. Am.* **28**, 168–191 (1956).
- Hamdi, F. A. I. & Taylor Smith, D. *Geophys. Prospect.* **30**, 622–640 (1982).
- Geertsma, J. & Smith, D. C. *Geophysics* **26**, 169–181 (1961).
- Hamdi, F. A. I. & Taylor Smith, D. *Geophys. Prospect.* **29**, 715–729 (1981).
- Hamilton, E. L. *J. geophys. Res.* **75**, 4423–4445 (1970).
- Anderson, R. S. in *Physics of Sound in Marine Sediments* (ed. Hampton, L.), 481–518 (Plenum, New York, 1974).
- Morgan, N. A. *Geophysics* **34**, 529–545 (1969).
- Schultheiss, P. J. in *Acoustics and the Sea Bed* (ed. Pace, N. G.) 19–27 (Bath University Press, 1983).
- Schultheiss, P. J. *Marine Geotechnol.* **4**, 343–367 (1981).
- Hamilton, E. L. *Geophysics* **41**, 985–996 (1976).
- Ohta, V. & Goto, N. *Earthq. Engng struct. Dyn.* **6**, 167–187 (1978).

Deformation of till beneath ice stream B, West Antarctica

R. B. Alley, D. D. Blankenship,
C. R. Bentley & S. T. Rooney

Geophysical and Polar Research Center, University of Wisconsin-Madison, 1215 West Dayton Street, Madison, Wisconsin 53706, USA

The behaviour and possible instability of the West Antarctic ice sheet depend fundamentally on the dynamics of the large ice streams which drain it. Model calculations show that most ice-stream velocity arises at the bed^{1,2}, and radar sounding has shown the bed to be wet³, but the basal boundary condition is not well understood. Seismic evidence from the Upstream B camp (UpB) on the Siple Coast of West Antarctica⁴ shows that the ice stream there rests on a layer of unconsolidated sediment averaging 5 or 6 m thick, in which the water pressure is only $\sim 50 \text{ kPa}$ less than the overburden pressure. Because this thin layer occurs well inland beneath an active ice sheet and rests on a surface showing flutes⁴ characteristic of glacial erosion⁵, we presume that it is glacial till. We propose here that deformation within the till is the primary mechanism by which the ice stream moves, and we discuss implications of this hypothesis.

Three distinct lines of evidence relating to till porosity, force balance, and water balance indicate that the till at UpB is deforming; we present each of these here. First, lodged basal till has a porosity of $\leq 30\%$, whereas deformation of till causes dilation and porosity of $\sim 40\%$ (refs 6–8). The seismically determined porosity of $\sim 40\%$ for till at UpB⁴ is consistent with active deformation but too high for lodged till.

Second, we estimate that the basal shear stress is about twice the strength of till at UpB, so that the till should be deforming.